Journal of
Materials Chemistry A

Materials for energy and sustainability

Accepted Manuscript

This article can be cited before page numbers have been issued, to do this please use: H. Yu, Z. Zhang, J. Li, S. R. G. Balestra, Z. R. Gao and M. A. Camblor, *J. Mater. Chem. A*, 2026, DOI: 10.1039/D5TA06932G.

ROYAL SOCIETY OF CHEMISTRY

rsc.li/materials-a

View Article Online
DOI: 10.1039/D5TA06932G

ARTICLE

Unexpected Phase Selectivity in Germanosilicate Zeolite Synthesis: Discovery and Structure of HPM-18, a Novel Stable *d4r*-Containing Structure

Received 00th January 20xx,
Accepted 00th January 20xx

DOI: 10.1039/x0xx00000x

Huajian Yu,[a,b] Zhenghan Zhang,[c] Jian Li,[c] Salvador R. G. Balestra,[d] Zihao Rei Gao,*[a,e] and Miguel A. Camblor*[a]

For pure-silica zeolites containing double 4-rings (*d4r*) units it is generally expected that zeolite solid solutions can form across the full range of Si-Ge compositions. This is because *d4r* units, though strained in pure-silica compositions, are stabilized by Ge atoms at their corners. In this work, we show that using 1,3,4-trimethylimidazolium and fluoride as structure-directing agents, the phase selectivity of crystallization shifts from zeolite **ITW** at pure-silica compositions to a new zeolite, HPM-18, at low Ge fraction (0.15). HPM-18 contains the same *d4r* density as **ITW** and the same T-site fraction belonging to d4r, but is significantly more porous and less dense, making this phase selectivity change unexpected. Interestingly, while the structure of HPM-18 is ordered at low Ge fraction, increasing Ge fraction introduces two dimensional correlated disorder, and up to five different ordered polymorphs can be identified in the resulting intergrowth materials. We report synthesis, structural characterization and energy minimization calculations that explain these findings. An energy penalty for Si/Ge substitution in **ITW** explains the phase selectivity change, while reduced energy differences between HPM-18 polymorphs in GeO_2 compositions account for the increased disorder.

Introduction

Zeolites are crystalline microporous (alumino)silicates that find a wide range of applications in many industrial processes, including catalysis,[1] adsorption and separation processes,[2] and cation-exchange applications.[3] Their three-dimensional framework structures, composed of corner-sharing TO_4 tetrahedra (where T is typically Si or Al but are in occasions other atoms), contain pore systems with well-defined molecular dimensions due to the crystalline nature of zeolites. The properties of zeolites, typically a high surface area, molecular sieving capabilities, cation exchange properties and tuneable acidity, make them outperform other materials in numerous applications that go from oil refining to gas adsorption/separation and environmental remediation.[4-8]

The synthesis of zeolites is a complex and still not well-understood process governed by many interacting factors, among which the use of the so-called organic structure-directing agents (OSDAs) typically play a key role.[9] These organic molecules, frequently cations, interact with the inorganic species during the crystallization, determining in some extent the final zeolite structure and ending up occluded in its pores and cages.[10] The concept of structure direction has been fundamental in furthering the development of zeolite science, allowing for the discovery of many new framework types and new zeolite compositions as well as for the optimization of existing zeolites for specific applications.[11] Inorganic structure directing agents also exist. Among them, the use of some heteroatoms (T atoms other than silicon that can occupy tetrahedral framework positions) and of fluoride (a catalyst of the breaking and formation of T-O-T bonds) are of particular importance. The incorporation of Ge into zeolite frameworks has opened up new possibilities in zeolite synthesis.[12] Larger Ge ionic radius and more flexible Ge-O-Ge angles compared to silicon allow for the stabilization of certain structural units, particularly double four-ring (*d4r*) units, which are strained in pure silica compositions.[13] The fluoride route, which involves the use of fluoride anions as mineralizing agents, has been particularly successful in allowing to synthesize high-silica zeolites with reduced framework defects, including *d4r* structures, especially in highly concentrated conditions.[14,15]

[a] Mr. H. Yu, Dr. Z. R. Gao, and Prof. M. A. Camblor
Instituto de Ciencia de Materiales de Madrid (ICMM), CSIC
C/ Sor Juana Ines de la Cruz, 3, 28049 Madrid, Spain
E-mail: macamblor@icmm.csic.es
[b] Mr. H. Yu
Escuela de Doctorado, Universidad Autónoma de Madrid, Madrid 28049, Spain
[c] Mr. Z. Zhang, and Prof. J. Li
State Key Laboratory of Coordination Chemistry, School of Chemistry and Chemical Engineering, Nanjing University, Nanjing 210023, China.
[d] Dr. S. R. G. Balestra
Departamento de Física Atómica, Molecular y Nuclear, Área de Física Teórica, Universidad de Sevilla
Av. Reina Mercedes s/n, 41012 Seville, Spain.
[e] Dr. Z. R. Gao
Department of Chemical and Biomolecular Engineering and Institute for NanoBioTechnology, Johns Hopkins University
3400 N Charles St., Baltimore, MD 21218, the USA
E-mail: zgao44@jhu.edu

Supplementary Information available: The authors have cited additional references within the Electronic Supplementary Information (ESI).[49-54] Experimental section, tables of synthesis results, crystallographic data, enumeration of HPM-18 polymorphs, and cRED, PXRD and FESEM images are included in the ESI. See DOI: 10.1039/x0xx00000x

View Article Online
DOI: 10.1039/D5TA06032C

According to calculations by Zicovich Wilson and co-workers, occlusion of fluoride in *d4r* units makes the framework more flexible by decreasing the covalent character, hence directionality, of the Si-O bond.[16,17] This makes pure silica structures containing *d4r* reachable for crystallization, despite their strained nature. Calcination of the zeolite removes the occluded fluoride, alongside the OSDA, and typically renders an essentially perfect, defect-free, SiO_2 framework.[18,19]

Although germanosilicates with high Ge content often exhibit limited hydrothermal stability, they remain of significant interest to researchers for two key reasons. Firstly, these materials can frequently be utilized in the Assembly-Disassembly-Organization-Reassembly (ADOR) process, leading to the creation of novel zeolitic materials with unique structural features and an improved stability.[20-22] The ADOR process takes advantage of the chemical weakness in Ge-rich frameworks to selectively disassemble and then reassemble the structure, often resulting in new zeolite topologies that are unattainable through direct traditional synthesis routes.[23] Secondly, newly discovered structures that are firstly obtained as germanosilicates can serve as targets for the design of new organic structure-directing agents (OSDAs) that could potentially yield these frameworks in more stable, low-germanium high-silica compositions.[24] Thus, both approaches have the potential to expand the range of accessible zeolite structures while improving their stability and applicability. Additionally, post-synthesis methods can convert unstable germanosilicates into stable materials with lower Ge content.[25-27]

For pure-silica zeolite structures containing *d4r* units, such as **ITW**,[28] one could expect that it should be possible to prepare zeolite solid solutions across the entire range of Ge fractions (Ge_f = Ge/(Ge+Si) from 0 to 1) using the fluoride route. This expectation stems from the known affinity of both fluoride and germanium atoms for *d4r* units, which should in principle stabilize these structures across all Ge-Si compositions. This for instance, has been shown to be the case for zeolite **STW**, also containing *d4r,* which we have synthesized in the whole range from pure silica to pure germania.[29,30] Examples with the **AST** framework type also exists.[31] However, in this work, we report a surprising finding that challenges the above assumption. Using 1,3,4-trimethylimidazolium (134TMI) as the OSDA and fluoride anions as mineralizing agents, i.e. the structure directing agents first used to discover **ITW**,[32] we observed a dramatic shift in phase selectivity from **ITW** to a new zeolite structure, designated as HPM-18 (zeolite number 18 from the Nanostructured Hybrid Biohybrid and Porous Materials group of ICMM, Madrid), at a remarkably low Ge fraction of just 0.15. Intriguingly, HPM-18 contains the same density of *d4r* units as **ITW** (one *d4r* per 12 T atoms) and an identical fraction of T sites belonging to *d4r* (2/3 of T sites). This unexpected change in phase selectivity at such a low germanium content is particularly perplexing, given the structural similarities between **ITW** and HPM-18 in terms of their *d4r* content. **ITW** possesses a relatively simple framework with a 2D system of pores defined by rings containing 8 $SiO_{4/2}$ tetrahedra, i.e. 8R pores, while the structure of HPM-18 is pretty complex and less dense and features a rather intricate system of pores: 12R, 8R and 7R pores run along one crystallographic direction (*b*) while a second pore will be described below. Thus, HPM-18 is a new addition to the scarce "odd zeolites", i.e. those zeolites that contain odd-membered pores,[33] a class of zeolites that constitutes less than 5% of all the ordered zeolite framework types recognized by the Structure Commission of the International Zeolite Association.[34] HPM-18 contains in fact rings with all possible number of atoms from 4 to 12. Additionally, we show here that HPM-18 can also be synthesized with higher Ge_f and in that case we observe two dimensional correlated disorder and up to five different polymorphs have been identified. Thus, it is only the third odd zeolite that can be a disordered intergrowth of different polymorphs, after EMM-17 and HPM-14.[35,36] These three intergrown odd zeolites possess different odd pores: 11R in EMM-17, 9R in HPM-14, and 7R in HPM-18.

Here, we present a comprehensive study of the synthesis, structural characterization, and energetics of HPM-18. Our aim, in addition to reporting a new zeolite structure, is to get insights on the underlying factors driving this unexpected phase selectivity and to contribute to a deeper understanding of the complex interplay between composition, structure direction, and framework energetics in zeolite crystallization. This investigation not only introduces a novel zeolite but also objects to our current understanding of structure direction in germanosilicate zeolite synthesis, potentially contributing to opening new strategies for the discovery of new zeolites.

Results and Discussion

Zeolite synthesis and physicochemical characterization of HPM-18

Table 1. Chemical composition of HPM-18.

	wt%			Molar ratio[b]		wt%[c]	
Ge_f[a]	N	C	H	C/N	H/N	TG residue	Unit cell[d]
0.17	3.13	8.68	1.96	3.24	8.69	81.5 (79.0)	$(C_6N_2H_{11}F)_{4.59}(H_2O)_{14.64}[Si_{39.84}Ge_{8.16}O_{96}]$
0.35	3.29	8.53	1.74	3.03	7.34	82.7 (80.8)	$(C_6N_2H_{11}F)_{5.28}(H_2O)_{9.71}[Si_{31.2}Ge_{16.8}O_{96}]$
0.63	3.29	8.39	1.68	2.98	7.09	82.7 (81.3)	$(C_6N_2H_{11}F)_{6.11}(H_2O)_{9.71}[Si_{17.76}Ge_{30.24}O_{96}]$
0.78	3.07	7.65	1.53	2.91	6.93	84.0 (82.9)	$(C_6N_2H_{11}F)_{6.02}(H_2O)_{8.60}[Si_{10.56}Ge_{37.44}O_{96}]$

[a] By EDS. [b] The ratios in pristine134TMI are C/N=3.0 and H/N=5.5. [c] The value calculated for the composition in the last column appears between parentheses. [d] OSDAF calculated from the N content, water from the excess H.

View Article Online
DOI: 10.1039/D5TA06932G

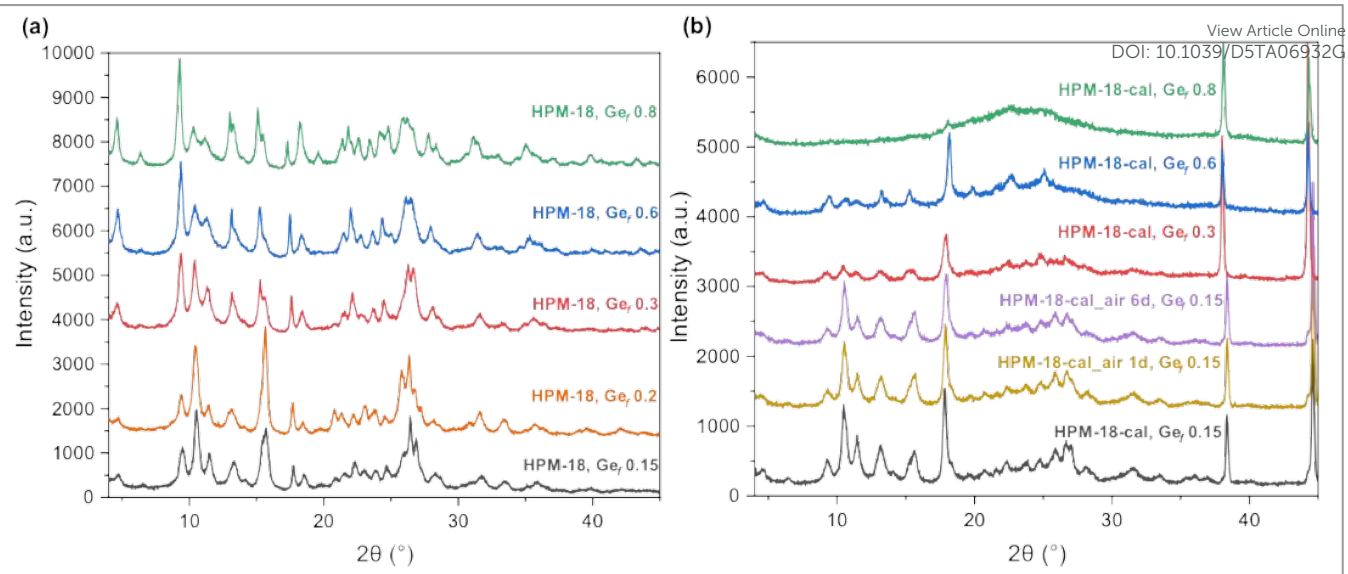

Figure 1. PXRD patterns of (a) five as-made HPM-18 with different Ge_f in gel (from bottom: 0.15, 0.2, 0.3, 0.6 and 0.8) and (b) calcined HPM-18 (from bottom to top: calcined HPM-18 (Ge_f 0.15), calcined HPM-18 exposed to ambient air for 1 d and 6 d; calcined HPM-18 (Ge_f 0.3) and calcined HPM-18 (Ge_f 0.6) respectively). Two peaks around 37.5° and 45° in (b) belong to the Aluminum sample holder.

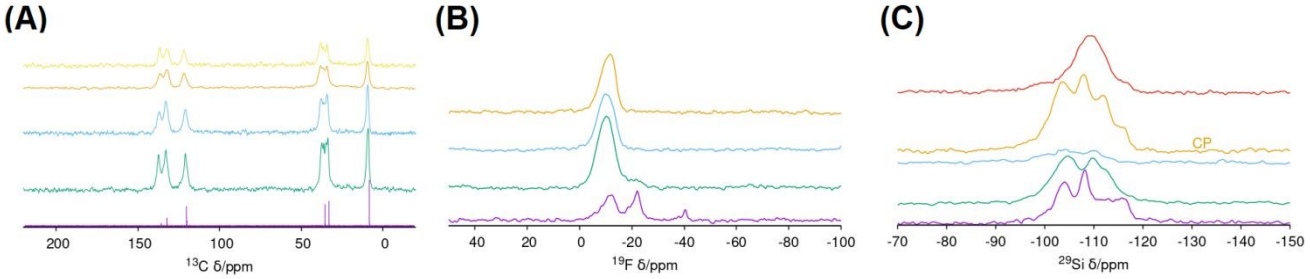

Figure 2. MAS NMR study of HPM-18: (A) ^{13}C MAS NMR spectrum of HPM-18 with (from top) Ge_f = 0.8, 0.6, 0.3 and 0.17 and ^{13}C NMR in D_2O of 134TMI iodide (bottom); (B) ^{19}F MAS NMR spectra of HPM-18 samples synthesized from gels with Ge_f = 0.1 (bottom), 0.3, 0.6 and 0.8 (top); (C) ^{29}Si MAS NMR spectra of HPM-18 (from bottom) with Ge_f = 0.17, 0.3, 0.6 and ^{29}Si $\{^1H\}$ CP MAS NMR of the sample with Ge_f = 0.17 and ^{29}Si MAS NMR spectrum of calcined HPM-18 (Ge_f = 0.17).

In the absence of Ge, 134TMI structure-directs the crystallization of pure silica **ITW**,[32] although under certain conditions **TON** may crystallize first and then recrystallize into the more porous and less stable (in the absence of guests) **ITW**.[37] That is a quite unique example of stability reversal by host-guest interactions. Among the three small imidazolium cations known to act as OSDAs for pure silica **ITW**, 134TMI has been rated as the worst OSDA.[17] When Ge is introduced in the crystallizing medium other phases start to compete (Table S1). For a Ge_f = 0.1, **ITW** still dominates the crystallization field but at the higher concentration tried (H_2O/SiO_2 = 1) some competition with HPM-18 already occurs. Upon further increasing the Ge_f the crystallization of HPM-18 is clearly favored, although a significant dependency on the water content is also observed. For instance at a Ge_f = 0.15 we obtained pure HPM-18 at high concentration and pure **ITW** at low concentration (H_2O/SiO_2 = 2.5 and 6, respectively). A further increase of Ge_f to 0.2 favors HPM-18 *vs* **ITW** and at 0.3 the competition is between HPM-18 (again favored at high concentration) and a phase of the disordered IM-18 family.[38] The presence of IM-18, which can be detected by two sharp peaks around 7.7 and 15.7° and a broad one around 8.7°, is more prominent as the degree of dilution increases (Figure S6). At a Ge_f of 0.6 and 0.8 the only crystalline phase obtained is HPM-18 for any H_2O/SiO_2 ratio tried, while at a pure germanate composition dense GeO_2 was obtained. These results clearly suggest that Ge favors HPM-18 vs **ITW** or IM-18 and at low Ge_f HPM-18 is favored at high concentration. As derived from the structural analysis below, the experimental framework density (FD expressed in this paper always as T atoms per 1000Å^3) of calcined HPM-18 (17.00 for a Ge_f = 0.17) is considerably lower than that of calcined ITW (18.15, Ge_f = 0)[28] and as-made 4-dimethylaminopyridine-IM-18 (17.85 for Ge_f =0.32). Despite the fact that there certainly must be an influence of both Ge_f and the presence of occluded guests on the calculated FD, so that the above FDs are not directly and exactly comparable, we find it very likely that HPM-18 is the least dense of the three phases in question here. This suggests that our empirical observations agree with the Villaescusa's rule, which was derived from observations of purely siliceous zeolite systems and states that, in fluoride media, the less dense phases are favored the higher the concentration.[14] The plausible applicability of the

View Article Online DOI: 10.1039/D5TA06972G

Villaescusa rule to germanosilicate zeolites had been recently proposed.[39]

Figure 1 shows the PXRD patterns of HPM-18 synthesized from gels with Ge_f from 0.15 to 0.8. All the as-made materials show a good crystallinity (Figure 1a), while peak positions and relative intensities vary as the Ge_f changes. However, after calcination (Figure 1b) samples with Ge_f of 0.3 or higher show an evident structural degradation right after calcination. On the contrary, for the sample with Ge_f = 0.17 the structural integrity is maintained even after exposure to ambient air for 6 days. Ar adsorption/desorption isotherms on that calcined sample revealed a specific surface area of 327 m^2g^{-1} (Figure S10) and the details are given in the ESI.

According to ^{13}C MAS NMR (Figure 2A) the OSDA is occluded intact in HPM-18. Chemical analysis suggests there are around 4 cations per unit cell of HPM-18 in the sample with less Ge (Table 1) and that the zeolite also contains a large amount of water. The excess OSDA observed in Table 1 is attributed to the difficulty in washing away OSDA occluded in the intercrystallite space. The ^{19}F MAS NMR spectra of HPM-18 with different Ge_f are shown in Figure 2B. All the samples show resonances in the range expected for fluoride occluded in *d4r* cages. We note here that samples that are incompletely washed may show a sharp resonance around -120 to -130 ppm, likely related to fluoride in F-Si bonds. The samples with more Ge show a strong resonance around -10/-11 ppm, i.e. type III corresponding to fluoride in *d4r* containing Ge pairs but not larger Ge clusters. This type of *d4r* can have between 2 and 6 Ge atoms.[30] The sample with Ge_f = 0.3 also contains a second small signal around -21 ppm, i.e. type II, corresponding to *d4r* containing non-paired Ge (which may contain between and 1 and 3 isolated Ge). By contrast, the sample with less Ge shows a resonance type I around -40 ppm as well as types II (-22 ppm) and III (-12 ppm). The ^{29}Si MAS NMR and $^{29}Si\{^1H\}$ CP are shown in Figure 2C and are typical of germanosilicates with varying Ge_f. Cross-polarization enhances all the resonances at lower field. After calcination only resonances in the -94/-120 ppm are observed, as expected for germanosilicate zeolites (Figure 2C, top).

cRED Structure Solution and Rietveld Refinement of Ordered Calcined HPM-18 of Ge_f 0.17

cRED data processing was carried out with the XDS software package. To enhance data completeness, several selected datasets for each sample were rescaled and merged using XSCALE (within the XDS suite), producing HKL files for subsequent structure solution and refinement. Following cRED data acquisition, the 3D reciprocal lattice was reconstructed using REDp, which facilitated indexing and identification of reflection conditions. The structure of HPM-18 was initially solved from the cRED data of a sample with a very high Ge_f (0.8). However, we suspected an effect of Ge_f on disorder from an analysis of the broadness of the reflection peaks: determination of the fwhm of the 3.3º peak of the SPXRD patterns of four samples with varying Ge_f shows that the fwhm sharply increases when the Ge_f increases from 0.17 to 0.6 (60% increase) and then slightly decreases for Ge_f = 0.8 (Figure S7). This occurs despite the fact that the size of the crystallites tends to increase continuously with the Ge_f (see Figure S8). Hence, two additional samples (Ge_f = 0.17 and 0.6) were studied by cRED in order to investigate the influence on Ge on disorder. cRED showed the presence of streaks in the samples with higher Ge_f, indicative of disorder (Figures S1-S3), but no streaks were detected in the sample with Ge_f = 0.17 (Figures S4-S5). For that sample, the structure of HPM-18 was determined ab initio using SHELXT, with the HKL file (containing reflection data) and P4P file (containing unit cell parameters) as inputs. This enabled direct localization of all framework atoms within the asymmetric unit, 24 T atoms and 48 O atoms. The final structure refinement was performed in Olex2 using electron-specific atomic scattering factors. Detailed crystallographic data obtained via cRED are provided in Tables S1-S2. The same procedure applied to the initial dataset collected from the sample with higher Ge_f afforded a solution corresponding to the average structure of a zeolite exhibiting a large degree of correlated 2D disorder arising from two possible locations of four of the *d4r* along the direction *b* (see below) of which the former ordered structure was a particular polymorph (polymorph D, see below).

An ordered polymorph model of HPM-18 with low Ge content was directly obtained from cRED data in *P*-1 (its maximum symmetry). This model was used as the initial structure for Rietveld refinement against synchrotron powder X-ray diffraction (SPXRD) data using Topas 5.0.[40] Prior to refinement, the framework geometry was optimized via the distance-least-squares (DLS) algorithm implemented in DLS-76,[41] and the SPXRD background was manually subtracted. In the initial refinement steps, soft restraints were applied to Si(Ge)-O bond lengths (1.61-1.72 Å), Si(Ge)-O-Si(Ge) angles (145°), and O-Si-O angles (109°). These restraints were gradually relaxed over several cycles. Additionally, the Si and Ge occupancies of each crystallographic T site were also refined, resulting in around 80 % of the Ge being located in d4r units and details are provided in the ESI. To account for anisotropic line broadening, a dedicated Topas macro contributed by Prof. Alan Coelho was employed.[42] The structure of ordered HPM-18 will be discussed below in relation to disorder and pore system. Crystallographic Tables (S4-S6) and the Rietveld plot (Figure S9) are provided in SI and the cif file has been deposited in the CCDC database (CCDC 2476607).[43]

Topology Analysis: Disorder and Polymorphs Extraction and HPM-18 Structure Description

In the average structure obtained from cRED of the highest Ge_f material there are four *d4r* per unit cell with a half occupancy and another two *d4r* that are completely ordered (Figure 3). Looking down [010] disorder is observed around positions A (0.25a, 0.25c), B (0.25a, 0.75c), C (0.75a, 0.25c) and D (0.75a, 0.75c). At each position, the *d4r* can be located either at the top (*b* = 0.5-1, marked as circle in Table S7) or at the bottom (*b* = 0-0.5, marked as crosses in Table S7) half of the unit cell. The top and the bottom positions are mutually exclusive, meaning that if the top space were occupied by a *d4r*, then the bottom space must remain unoccupied, and vice versa, resulting in correlated

Journal Name ARTICLE

View Article Online
DOI: 10.1039/D5TA06932G

disorder. The unoccupied space is a cage occupied by the OSDAs in the as-made form of HPM-18. However, the sequence (top or bottom) of the *d4r* at one position does not determine the sequences at the other positions. This means that each unit cell has four independent variables determining the position of the *d4r*s. In other words, there are four independent possibilities controlling whether the d4r occupies the top or bottom position at each site (A to D). The disorder observed in HPM-18 high Ge

View Article Online
DOI: 10.1039/D5TA06932G

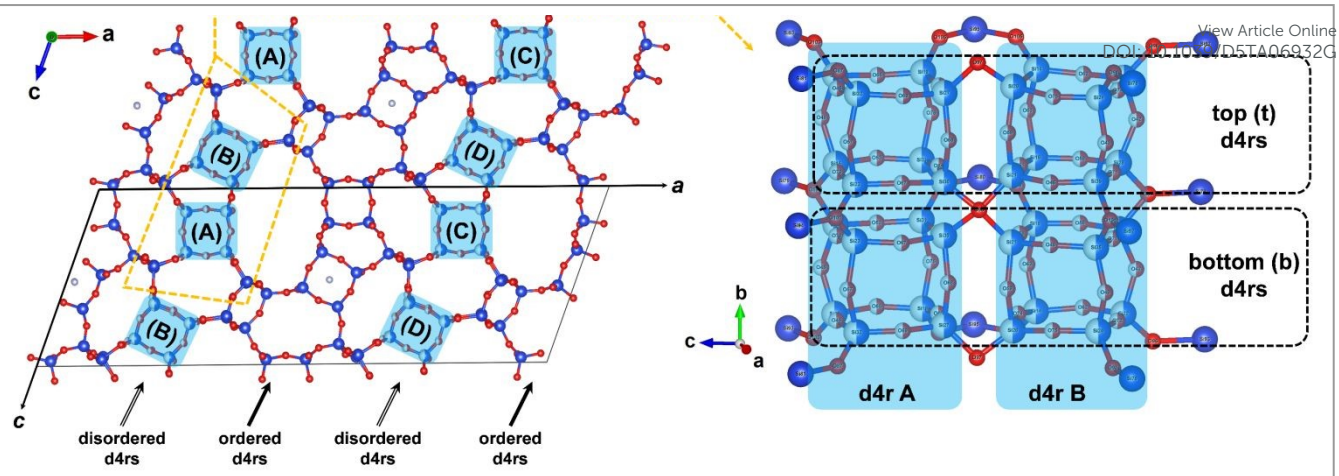

Figure 3. Structure of HPM-18 with correlated disorder of four *d4r* (highlighted in blue), viewed along [010] direction, (left) and the top/bottom possible positions of *d4r* at positions A and B, viewed along approximately [101] direction (right). The T and O atoms from the disordered *d4r* are shown as half-occupied blue and red spheres, respectively, while the other T sites and O atoms are depicted as full occupied blue and red spheres. The structure at the right corresponds with the orange dash frame at the left and the top and bottom positions are mutually exclusive.

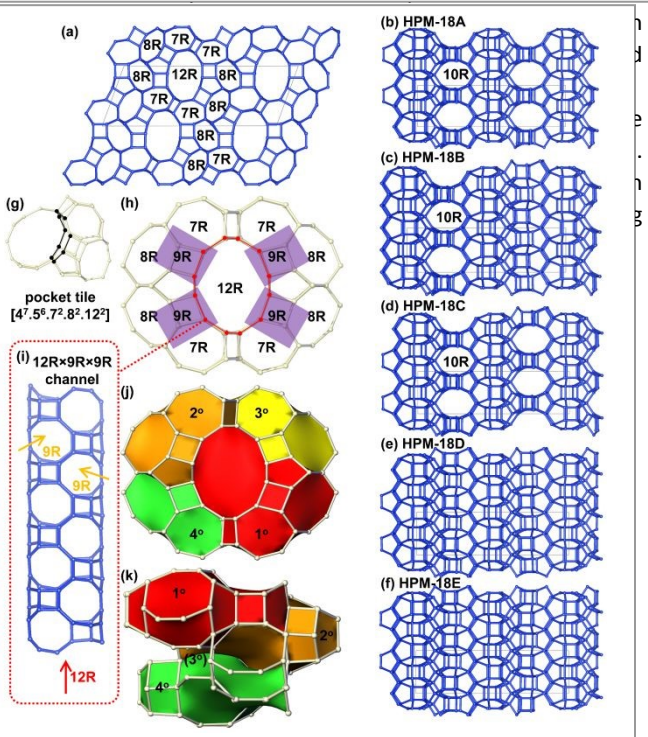

Figure 4. Structure of HPM-18: (a) viewed along the [010] direction showing the straight 12R, 8R, and 7R channels; (b-f) HPM-18 polymorphs A-E viewed along the [001] direction, showing straight 10R in polymorphs A-C and the absence of straight 10R channels in polymorph D-E (where undulating 10R exist instead); (g) a large pocket-like tile [$4^7.5^6.7^2.8^2.12^2$] present in all polymorphs; (h) 4 pocket-like tiles; (i) straight 12R channels with 9R pore stretches openning to the 4 pockets, (j) stacking sequence of 4 pockets (red-orange-yellow-green) along the [010] direction; (k) viewed through the yellow pocket to show the 9R pore connecting the 12R and 8R channels.

the 12R channel shown in Figure 4h. The stacking sequence is illustrated in Figure 4j as red-orange-yellow-green stacking down along the b-axis. For instance, the red tile is rotated into the orientation of the orange tile with a -1/4b shift. This combination of rotation and translation along the b-axis is repeated to build the structure shown in Figure 4j. When Figure 4j is viewed from another direction, with the yellow tile removed for clarity, the resulting structure is shown in Figure 4k, revealing that 9R pore stretches exist at the intersections of the 12R straight channels and the pockets (Figure 4i). Topology analysis also indicates that HPM-18 contains de facto rings with all possible number of atoms from 4 to 12. However, only 4R, 5R, 7R, 8R, and 12R are considered as "strong rings", i.e. they are rings that are not the sum of smaller rings. As a result, HPM-18E possesses a 3D 12x8x8 R channel system, with additional 7R and 8R channels aligned in the same direction as the 12R channel.

Site-Occupancy Disorder and Stability of ITW and HPM-18

For each HPM-18 polymorph as well as for ITW we generated structures with full occupancies of T (as Si or Ge) and O sites, and the structures were energy minimised. Table 2 shows the enthalpy results for the five polymorphs and ITW zeolites as SiO_2 and GeO_2 compositions. For pure silicate zeolites the most stable zeolite is **ITW**. The enthalpic order for the HPM-18 polymorphs is E > D > B > A > C, with relative enthalpies with respect to the most stable phase of 0.14 (D), 1.51 (B), 2.79 (A), and 2.81 (C) kJ mol^{-1}. Regarding GeO_2 compositions, all HPM-18 polymorphs are more stable than **ITW**. The stability order is the same as for SiO_2 compositions but with relative enthalpies of 0.19 (D), 0.66 (B), 1.17 (A), and 1.41 (C) kJ mol^{-1}. It is important to note, first, that the most stable HPM-18 polymorph E is the one that arose from the structural model obtained from cRED data at low Ge content, and also the one successfully used in the Rietveld refinement of that zeolite. Second, the energy span in Table 2 is much larger at the SiO_2 side (5.26 kJ mol^{-1}) than at the GeO_2 side (1.42 kJ mol^{-1}). Third, there is a significant energy penalty associated with the substitution of Si by Ge in ITW (over 4 kJ mol^{-1}), while in HPM-18 that substitution implies either a small penalty (0.02-0.88 kJ mol^{-1} for the most stable polymorphs) or a small benefit (-0.5 to -0.72 kJ mol^{-1} for the less stable polymorphs A and C). These calculations help to rationalise the observed structure-direction change from ITW to HPM-18 at low Ge fractions (due to the significant penalty of Si by Ge substitution in **ITW**), and they also indicate that the convergence of polymorph energies at high Ge content increases the relevance of entropic contributions, favouring disorder and intergrowth.

The energy minimisation calculations above provide insights into the relative thermodynamic stability of the five HPM-18 polymorphs and **ITW**, but they were performed for pure SiO_2 and GeO_2 compositions. Direct comparisons across compositions must therefore be interpreted with caution due to the differing chemical environments and bonding preferences of Si and Ge. A more rigorous approach involving enthalpies or formation energies for intermediate compositions could, in principle, provide a more complete view of the energetic landscape. For this reason, we have examined instead the evolution of the ensemble-averaged Gibbs energy, ⟨Δg⟩, with respect to the Ge fraction (Ge_f), primarily for the **ITW** and HPM-18-E frameworks across the full compositional range. To achieve this, we developed a modified version of the SOD code tailored to this system (see ESI). In addition, both OSDA cations and F^- anions were explicitly included in all energy optimisations, as detailed in the methodological section of the ESI.

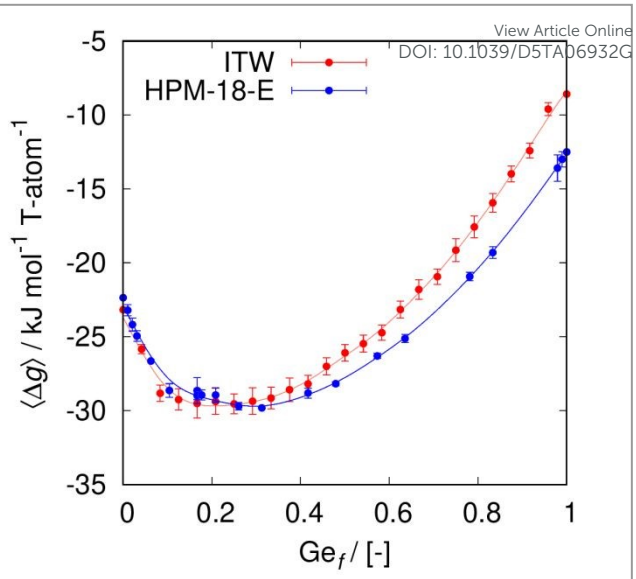

Figure 5. Calculated ⟨Δg⟩ ensemble-averaged Gibbs energies per T-atom relative to a linear combination of quartz SiO_2 and quartz-type GeO_2 (for $Ge_xSi_{1-x}O_2$ compositions) at 150 °C, and hypothetical 134TMI$^+$F$^-$ salt, for ITW (red) and HPM-18-E (blue) zeolites. See ESI for the estimation of error bars. Solid lines represent spline interpolations of the free energy data, included solely to guide the eye.

Table 2. Calculated enthalpy per T-atom with respect to SiO_2 or GeO_2 quartz, Δh, for HPM-18 polymorphs and ITW zeolites. In bold numbers, we have highlighted the most stable zeolite for SiO_2 and GeO_2 compositions.

	Δh / [kJ mol^{-1}]	
	SiO_2	GeO_2
HPM-18A	14.02	19.23
HPM-18B	12.71	18.71
HPM-18C	14.00	19.47
HPM-18D	11.34	18.24
HPM-18E	11.20	**18.05**
ITW	**8.76**	18.82
span ($\Delta\Delta h$) [a]	5.26	1.42

[a] span (ΔΔh) is the enthalpy difference between the highest and lowest calculated energies in each column.

View Article Online
DOI: 10.1039/D5TA06952G

As shown in Figure 5, introducing Ge into ITW stabilises the framework at very low Ge_f values, but leads to destabilisation at higher fractions (ca. Ge_f ~ 0.2) relative to the HPM-18-E framework. Although the HPM-18-E structure has a higher enthalpy than ITW, the increasing mixing entropy as Ge_f grows, together with an additional configurational contribution associated with polymorphism (ca. -5.45 and -5.62 kJ mol^{-1} for the Ge_f = 0 and Ge_f = 1 values, respectively), results in a substantial decrease in Gibbs energy and enhances the stability of the polymorph mixture. This polymorph entropy corresponds to the configurational contribution arising from the number of distinct polymorphs accessible at a given Gef, as detailed in the ESI. So, when the configurational entropy is incorporated into the analysis, the thermodynamic picture becomes fully consistent with the experimentally observed disorder: as the polymorphs approach energetic degeneracy at high Ge content, the system favours disordered intergrowths that maximise configurational entropy, manifested experimentally as streaks in cRED data and peak broadening in PXRD patterns.

These results reinforce the conclusions obtained from the enthalpy analysis and help explain why the phase selectivity of the crystallisation shifts from **ITW** to HPM-18 at relatively low Ge contents. In addition, vibrational entropy may contribute to the overall disorder and the evolution of phase selectivity, although the present analysis accounts only for the configurational component (mixing and polymorph entropies). Vibrational effects are expected to be smaller in magnitude but could further modulate the free-energy balance, particularly at elevated temperatures.

Conclusions

In this work, we report the discovery and structural characterization of HPM-18, a novel germanosilicate zeolite featuring double four-ring (*d4r*) units and an unusual phase selectivity behavior in its synthesis. Contrary to our expectations based on previous structure-directing observations, the use of 1,3,4-trimethylimidazolium (134TMI) and fluoride ions led to the crystallization of HPM-18 at a low Ge fraction (Ge_f = 0.15 in the gel), instead of the anticipated and denser **ITW** phase, while **ITW** is the predominant phase at pure silica compositions. This finding challenges the assumption that *d4r*-containing frameworks like **ITW** should be favored across the full Ge-Si compositional range under fluoride-mediated conditions. The structure of HPM-18 has been solved from cRED data. It exhibits a complex pore system containing both even and odd-membered rings and can be synthesized over a wide range of Ge contents. However, while at very low Ge_f the structure is ordered and is coincident with the most stable polymorph E, at high Ge fractions the structure displays two-dimensional correlated disorder, resulting in an intergrowth of multiple possible polymorphs. The ordered structure has been Rietveld refined using SPXRD. HPM-18 has a lower framework density than **ITW** and IM-18 and is favored at high concentrations, consistent with the empirical Villaescusa's rule, which correlates phase selectivity with framework density and concentration in fluoride media. Calculations suggest a large penalty for substituting Si by Ge in **ITW**, which would be the cause for the observed structure-direction change at low Ge_f. They also indicate that the six HPM-18 polymorphs become increasingly similar in energy as the Ge content increases, providing an appreciable entropic contribution to the Gibbs energy at the synthesis temperature and, in turn, explaining the influence of Ge_f on the degree of structural order. The most stable HPM-18 is polymorph E.

Author contributions

HY: Conceptualization, supporting; Methodology, supporting; Validation, lead; Formal analysis, lead; Investigation, lead; Data curation, lead; Writing – Original Draft, supporting; Writing – Review & Editing, supporting. **ZZ**: Validation, lead; Formal analysis, supporting; Investigation, supporting; Data curation, lead; Writing – Review & Editing, supporting. **JL**: Methodology, supporting; Validation, supporting; Formal analysis, supporting; Investigation, supporting; Resources, supporting; Writing – Original Draft, supporting; Writing – Review & Editing, lead; Funding acquisition, supporting. **SRGB**: Software, lead; Validation, lead; Formal analysis, supporting; Investigation, supporting; Resources, supporting; Data curation, supporting; Writing – Original Draft, supporting; Writing – Review & Editing, lead; Visualization, supporting; Funding acquisition, supporting. **ZRG**: Conceptualization, lead; Methodology, lead; Investigation, supporting; Data curation, supporting; Writing – Original Draft, supporting; Writing – Review & Editing, lead; Visualization, lead; Supervision, supporting; Project administration, lead. **MAC**: Conceptualization, lead; Methodology, lead; Investigation, supporting; Resources, lead; Data curation, supporting; Writing – Original Draft, lead; Writing – Review & Editing, lead; Supervision, lead; Project administration, lead; Funding acquisition, lead.

Conflicts of interest

There are no conflicts to declare.

Data availability

Crystallographic data for HPM-18 have been deposited at the CCDC under codes 2476607 (Rietveld) and 2473072 (cRED) and can be obtained from https://www.ccdc.cam.ac.uk/structures/. Other data for this article, including multinuclear MAS NMR, XRD and calculated energy data are available at ZENODO at https://doi.org/10.5281/zenodo.16949065.

Acknowledgements

Financial support from the Spanish Ministry of Science Innovation (PID2022-137889OB-I00, TED2021-131223B-I00, MCIN/AEI/10.13039/501100011033) is gratefully acknowledged. Synchrotron powder X-ray diffraction data experiments were performed at the Materials Science Powder Diffraction beamline bl04 at the ALBA Spanish Synchrotron with

View Article Online
DOI: 10.1039/D5TA06352G

the collaboration of the ALBA staff. H.Y. is grateful to the China Scholarship Council for a PhD grant. S.R.G.B. acknowledges grant RYC2022-036070-I funded by MICIU/AEI/10.13039/501100011033 and by "ESF+". Authors would like to thank the computing time provided by the Servicio de Supercomputación de la Universidad de Granada. We acknowledge the Severo Ochoa Centres of Excellence program through Grant CEX2024-001445-S.

Notes and references

1 H. Zhang, I. bin Samsudin, S, Jaenicke, G.-K. Chuah, "Zeolites in Catalysis: Sustainable Synthesis and Its Impact on Properties and Applications." *Catal. Sci. Technol.* **2022**, 12 (19), 6024–6039.

2 K. Chen, S. H. Mousavi, R. Singh, R. Q. Snurr, G. Li, P. A. Webley, "Gating Effect for Gas Adsorption in Microporous Materials—Mechanisms and Applications." *Chem. Soc. Rev.* **2022**, 51 (3), 1139–1166.

3 E. Koohsaryan, M. Anbia, M. Maghsoodlu, "Application of Zeolites as Non-phosphate Detergent Builders: A Review." *J. Envir. Chem. Eng.* **2020**, 8 (5), 104287.

4 T. F. Degnan, "Applications of Zeolites in Petroleum Refining." *Top. Catal.* **2000**, 13 (4), 349–356.

5 X. Han, W. Xu, F. Meng, Z. Liu, C. Liao, "Recent Advances in Zeolite Membranes for Gas Separation and Pervaporation in Petrochemicals." *J. Mater. Chem. A* **2025**, 13, 10358-10387.

6 I. Kabalan, B. Lebeau, H. Nouali, J. Toufaily, T. Hamieh, B. Koubaissy, J. P. Bellat, T. J. Daou, "New Generation of Zeolite Materials for Environmental Applications." *J. Phys. Chem. C* **2016**, 120, 5, 2688–2697.

7 Y. Li, L. Li, J. Yu, "Applications of Zeolites in Sustainable Chemistry." *Chem* **2017**, 3 (6), 928–949.

8 D. Kalló, "Applications of Natural Zeolites in Water and Wastewater Treatment." *Rev. Miner Geochem.* **2001**, 45, 519-550.

9 L. Gómez-Hortigüela, M. A. Camblor in *In Insights into the Chemistry of Organic Structure-Directing Agents in the Synthesis of Zeolitic Materials*, (Eds.: L. Gómez-Hortigüela), Springer International Publishing: Cham, **2018**, pp 1-41.

10 M. E. Davis, R. F. Lobo, "Zeolite and Molecular Sieve Synthesis." *Chem. Mater.* **1992**, 4 (4), 756–768.

11 A. W. Burton, S. I. Zones, S. Elomari, "The Chemistry of Phase Selectivity in the Synthesis of High-Silica Zeolites." *Curr. Opin. Colloid Interface Sci.* **2005**, 10 (5), 211–219.

12 M. A. Camblor, S. B. Hong in *Synthetic Silicate Zeolites: Diverse Materials Accessible Through Geoinspirationin Porous Materials*, (Eds: D. W. Bruce, D. O'Hare, R. I. Walton), Inorganic Materials Series; Wiley: Chichester, **2011**, pp 265–325.

13 T. Blasco, A. Corma, M. J. Díaz-Cabañas, F. Rey, J. A. Vidal-Moya, C. M. Zicovich-Wilson, "Preferential Location of Ge in the Double Four-Membered Ring Units of ITQ-7 Zeolite." *J. Phys. Chem. B* **2002**, 106 (10), 2634–2642.

14 M. Camblor, L. Villaescusa, M. Diaz-Cabanas, "Synthesis of All-Silica and High-Silica Molecular Sieves in Fluoride Media." *Top. Catal.* **1999**, 9, 59–76.

15 M. Camblor, P. Barrett, M. Diaz-Cabanas, L. Villaescusa, M. Puche, T. Boix, E. Perez, H. Koller, "High Silica Zeolites with Three-Dimensional Systems of Large Pore Channels." *Microporous Mesoporous Mater.* **2001**, 48, 11–22.

16 C. M. Zicovich-Wilson, M. L. San-Roman, M. A. Camblor, F. Pascale, J. S. Durand-Niconoff, "Structure, Vibrational Analysis, and Insights into Host-Guest Interactions in As-Synthesized Pure Silica ITQ-12 Zeolite by Periodic B3LYP Calculations." *J. Am. Chem. Soc.* **2007**, 129 (37), 11512–11523.

17 A. Rojas, E. Martinez-Morales, C. M. Zicovich-Wilson, M. A. Camblor, "Zeolite Synthesis in Fluoride Media: Structure Direction toward ITW by Small Methylimidazolium Cations." *J. Am. Chem. Soc.*, **2012**, 134 (4), 2255–2263.

18 L. Villaescusa, P. Barrett, M. A. Camblor, "Calcination of Octadecasil: Fluoride Removal and Symmetry of the Pure SiO2 Host." *Chem. Mater.* **1998**, 10 (12), 3966–3973.

19 C. M. Zicovich-Wilson, M. L. San Román, A. Ramírez-Solís, "Mechanism of F- Elimination from Zeolitic D4R Units: A Periodic B3LYP Study on the Octadecasil Zeolite." *J. Phys. Chem. C* **2010**, 114 (7), 2989–2995.

20 W. J. Roth, P. Nachtigall, R. E. Morris, P. S. Wheatley, V. R. Seymour, S. E. Ashbrook, P. Chlubná, L. Grajciar, M. Položij, A. Zukal, O. Shvets, J. Čejka, "A Family of Zeolites with Controlled Pore Size Prepared Using a Top-down Method." *Nat. Chem.* **2013**, 5, 628–633.

21 P. Eliášová, M. Opanasenko, P. S. Wheatley, M. Shamzhy, M. Mazur, P. Nachtigall, W. J. Roth, R. E. Morris, J. Čejka, "The ADOR Mechanism for the Synthesis of New Zeolites." *Chem. Soc. Rev.* **2015**, 44 (20), 7177–7206.

22 O. Veselý, R. E. Morris, J. Čejka, "Beyond Traditional Synthesis of Zeolites: The Impact of Germanosilicate Chemistry in the Search for New Materials." *Microporous Mesoporous Mater.* **2023**, 358, 112385.

23 M. Mazur, P. S. Wheatley, M. Navarro, W. J. Roth, M. Položij, A. Mayoral, P. Eliášová, P. Nachtigall, J. Čejka, R. E. Morris, "Synthesis of "unfeasible" Zeolites." *Nat. Chem.* **2016**, 8, 58–62.

24 F. Daeyaert, M. Deem, De Novo Design of Organic Structure Directing Agents for the Synthesis of Zeolites. In AI-Guided Design and Property Prediction for Zeolites and Nanoporous Materials, John Wiley & Sons, Ltd, **2023**, pp 33–59.

25 L. Burel, N. Kasian, A. Tuel, "Quasi All-Silica Zeolite Obtained by Isomorphous Degermanation of an As-Made Germanium-Containing Precursor." *Angew. Chem. Int. Ed.* **2014**, 53 (5), 1360–1363.

26 H. Xu, J. Jiang, B. Yang, L. Zhang, M. He, P. Wu, "Post-Synthesis Treatment Gives Highly Stable Siliceous Zeolites through the Isomorphous Substitution of Silicon for Germanium in Germanosilicates." *Angew. Chem. Int. Ed.* **2014**, 53, 1355-1359.

27 M. V. Shamzhy, P. Eliasová, D. Vitvarova, M. V. Opanasenko, D. S. Firth, R. E. Morris, "Post-Synthesis Stabilization of Germanosilicate Zeolites ITH, IWW, and UTL by Substitution of Ge for Al." *Chem. Eur. J.* **2016**, 22 (48), 17377–17386.

28 X. Yang, M. A. Camblor, Y. Lee, H. Liu, D. Olson, "Synthesis and Crystal Structure of As-Synthesized and Calcined Pure Silica Zeolite ITQ-12." *J. Am. Chem. Soc.* **2004**, 126 (33), 10403–10409.

29 A. Rojas, M. A. Camblor, "A Pure Silica Chiral Polymorph with Helical Pores." *Angew. Chem. Int. Ed.* **2012**, 51, 3854-3856.

30 R. T. Rigo, S. R. G. Balestra, S. Hamad, R. Bueno-Perez, A. R. Ruiz-Salvador, S. Calero, M. A. Camblor, "The Si-Ge Substitutional Series in the Chiral STW Zeolite Structure Type." *J. Mater. Chem. A* **2018**, 6 (31), 15110–15122.

31 Y. Wang, J. Song, H. Gies, "The Substitution of Germanium for Silicon in AST-Type Zeolite." *Solid State Sci.* **2003**, 5, 1421–1433.

32 P. Barrett, T. Boix, M. Puche, D. Olson, E. Jordan, H. Koller, M. A. Camblor, "ITQ-12: A New Microporous Silica Polymorph Potentially Useful for Light Hydrocarbon Separations." *Chem. Comm.* **2003**, 17, 2114–2115.

33 M. A. Camblor, M. Diaz-Cabanas, J. Perez-Pariente, S. Teat, W. Clegg, I. Shannon, P. Lightfoot, P. Wright, R. E. Morris, "SSZ-23: An Odd Zeolite with Pore Openings of Seven and Nine Tetrahedral Atoms." *Angew. Chem. Int. Ed.* **1998**, 37, 2122–2126.

34 Ch. Baerlocher, D. Brouwer, B. Marler, L. B. McCusker, "Database of Zeolite Structures", can be found under https://www.iza-structure.org/databases/, **2025** (accessed: 20/05/2025).

35 S. C. Weston, B. K. Peterson, J. E. Gatt, W. W. Lonergan, H. B. Vroman, M. Afeworki, G. J. Kennedy, D. L. Dorset, M. D. Shannon, K. G. Strohmaier, "EMM-17, a New Three-Dimensional Zeolite with Unique 11-Ring Channels and Superior Catalytic Isomerization Performance." *J. Am. Chem. Soc.* **2019**, 141 (40), 15910–15920.

36 Z. R. Gao, J. Li, C. Lin, A. Mayoral, J. Sun, M. A. Camblor, "HPM-14: A New Germanosilicate Zeolite with Interconnected Extra-Large Pores Plus Odd-Membered and Small Pores." *Angew. Chem. Int. Ed.*, **2021**, 60, 3438-3442.

37 C. M. Zicovich-Wilson, F. Gandara, A. Monge, M. A. Camblor, "In Situ Transformation of TON Silica Zeolite into the Less Dense ITW: Structure-Direction Overcoming Framework Instability in the Synthesis of SiO2 Zeolites." *J. Am. Chem. Soc.* **2010**, 132 (10), 3461–3471.

38 X. Wang, Y. Shen, R. Liu, X. Liu, C. Lin, D. Shi, Y. Chen, F. Liao, J. Lin, J. Sun, "Elucidation of Correlated Disorder in Zeolite IM-18." *Act. Crystallogr. B* **2019**, 75, 333-342.

39 P. Lu, L. A. Villaescusa, M. A. Camblor, "Driving the Crystallization of Zeolites." *Chem. Rec.* **2018**, 18, 713–723.

40 A. Coelho, "TOPAS and TOPAS-Academic: an optimization program integrating computer algebra and crystallographic objects written in C++." *J. Appl. Crystallogr.* **2018**, 51, 210-218.

41 C. Baerlocher, A. Hepp, W. M. Meier, W. M., DLS-76: A Program for the simulation of crystal structures by geometric refinement. Institute of crystallography and petrography, ETH Zurich, Zurich (Switzerland), **1976**.

42 "Topas wiki" can be found under https://topas.awh.durham.ac.uk/doku.php?id=anisotropic_hkl, **2025** (accessed: 20/03/25).

43 Deposition number 2476607 (for ordered HPM-18) contains the supplementary crystallographic data for this paper. These data are provided free of charge by the joint Cambridge Crystallographic Data Centre and Fachinformationszentrum Karlsruhe Access Structures service.

44 M. O. Cichocka, Y. Lorgouilloux, S. Smeets, J. Su, W. Wan, P. Caullet, N. Bats, L. B. McCusker, J.-L. Paillaud, X. Zou, "Multidimensional Disorder in Zeolite IM-18 Revealed by Combining Transmission Electron Microscopy and X-Ray Powder Diffraction Analyses." *Cryst. Growth Des.* **2018**, 18 (4), 2441–2451.

45 J. H. Kang, D. Xie, S. I. Zones, S. Smeets, L. B. McCusker, M. E. Davis, "Synthesis and Characterization of CIT-13, a Germanosilicate Molecular Sieve with Extra-Large Pore Openings." *Chem. Mater.* **2016**, 28, 6250–6259.

46 Z.-H. Gao, F.-J. Chen, L. Xu, L. Sun, Y. Xu, H.-B. Du, "A Stable Extra-Large-Pore Zeolite with Intersecting 14- and 10-Membered-Ring Channels." *Chem. Eur. J.* **2016**, 22, 14367–14372.

47 L. Xu, L. Zhang, J. Li, K. Muraoka, F. Peng, H. Xu, C. Lin, Z. Gao, J.-G. Jiang, W. Chaikittisilp, J. Sun, T. Okubo, P. Wu, "Crystallization of a Novel Germanosilicate ECNU-16 Provides Insights into the Space-Filling Effect on Zeolite Crystal Symmetry." *Chem. Eur. J.* **2018**, 24, 9247–9253.

48 "Intergrowth Family IM-18" can be found under https://america.iza-structure.org/IZA-SC/DO_structures/DO_family_scu.php?ID=14 , **2025** (accessed: 02/07/2025).

49 J. D. Gale, "GULP: A computer program for the symmetry-adapted simulation of solids." *J. Chem. Soc., Faraday Trans.* **1997**, 93, 629-637.

50 J. D. Gale, A. L. Rohl, "The General Utility Lattice Program (GULP)." *Mol. Simul.* **2003**, 29, 291-341.

51 G. Sastre J. Gale, "Derivation of an Interatomic Potential for Fluoride-Containing Microporous Silicates and Germanates", *Chem. Mater.* **2005**, 17, 4, 730–740

52 R. Grau-Crespo, S. Hamad, C. R. A. Catlow, N. H. de Leeuw, "Symmetry-adapted configurational modelling of fractional site occupancy in solids", *J. Phys. Condens. Matter* **2007**, 19, 256201.

53 R. Grau-Crespo, U. V. Waghmare in *Molecular Modeling for the Design of Novel Performance Chemicals and Materials*, (Ed.: B. Rai), CRC Press, **2012**, ch. 11.

54 J. Arce-Molina, R. Grau-Crespo, D. W. Lewis, A. R. Ruiz-Salvador, "Screening heteroatom distributions in zeotype materials using an effective Hamiltonian approach: the case of aluminogermanate PKU-9", *Phys. Chem. Chem. Phys.*, **2018**, 20, 18047-18055.

View Article Online
DOI: 10.1039/D5TA06932G

Crystallographic data for HPM-18 have been deposited at the CCDC under codes 2476607 (Rietveld) and 2473072 (cRED) and can be obtained from https://www.ccdc.cam.ac.uk/structures/.

Other data for this article, including multinuclear MAS NMR, XRD and calculated energy data are available at ZENODO at https://doi.org/10.5281/zenodo.16949065.